PSI-2981/
TR-2221

Self-Deployed Space or Planetary Habitats and Extremely Large Structures

Final Report
Covering the Period
1 September 2006 to 31 March 2007

University Space Research Association (USRA)
Subcontract No. 07605-003-059

NASA Institute for Advanced Concepts (NIAC)
Prime Contract No. NAS5-03110

Devon G. Crowe, Edward A. Reitman, Prakash B. Joshi, and Kophu Chiang

Physical Sciences, Inc.
20 New England Business Center
Andover, MA 01810-1077

June 2007

TABLE OF CONTENTS

LIST OF FIGURES

LIST OF FIGURES (Continued)

Phase I Summary

During Phase 1, PSI has demonstrated low mass bubble structures that can be fabricated by low-pressure inflation (~10^{-4} atmospheres) in a vacuum and then made rigid using solar UV curing. The surface density is on the order of one gram per square meter, enabling bubbles to enclose volume at system densities under 15 μg/cc. Space structures with volumes 10^8 times that of the spacecraft payload used to transport the materials become possible with this technology.

Phase 2 would include these tasks:

- Phase 2 is intended to combine Mission Designs with further laboratory development.
- Webster Cash has agreed to join the team for Phase 2 to integrate the concept into both the New Worlds Imager and one additional mission concept to be called Maxim.
- Antoine Labeyrie has contributed suggestions for large space telescope applications that include the Hypertelescope.
- One Phase 2 goal is to lay the foundation for flight missions for Block 2020.
- New Worlds Imager mission planning will be examined with the goal of incorporating low mass components to gain advantages that include:
    - More star shades in one launch for increased search rate by looking in one direction while other shades are maneuvering.
    - More Star shades for spares.
    - More star shades to serve more telescopes to increase the search set.
    - A lower mass, lower cost mission alternative.
    - The technology can also make lower mass mirrors of any conical and some non-conical shapes.
- Web Cash has another mission called Maxim in the planning stages that will also be included.

This technology would enable payloads small enough to launch that can become self-contained orbital habitats, large buildings on planetary surfaces, or other large structures that require significant strength. Our approach uses inflated bubble structures and suspended films which are then made rigid. Features of the approach include:

1. Bubbles and foam with individual cell sizes up to 100 meters
2. Structural spans can exceed 10,000 kilometers in micro-g environments
3. Structural densities as low as 15 μg/cc
4. Foam densities tessellate volume in a structured way to maximize density in regions of stress
5. Phononic crystals designed into the foam tailor the stiffness of structural members
6. In-situ bubble and foam formation and rigidization allows a deployed structure volume of up to 10^8 times the spacecraft volume that deploys it

Applications for these structures include:

1. Self-sustaining space habitats for extended duration uses
    a. Space stations
    b. Planetary expeditions
    c. Interstellar voyages.
2. Planetary surface buildings.
3. Astronomical telescope structures that replace formation flying requirements at very large scales
    a. Interferometer arrays
    b. Pinhole imagers
    c. Long focal length Fresnel plate telescopes.
4. Large area photon sails, stellar energy collectors, or astronomical primary photon collection surfaces
    a. Interstellar photon sailing
    b. Solar powered propulsion
    c. Laser propulsion at extreme ranges
    d. Beamed power transmission
    e. Photon perturbation of comet orbits for planetary protection
    f. Astronomical research on the origins of the universe and on evidence of life on planets within other solar systems
    g. Solar earth shade for global warming mitigation
    h. Optical apertures with tailored radius of curvature up to 100 meters in diameter
    i. Solar ablation of cometary surfaces to deflect NEO objects from earth-intersecting orbits for planetary defense.

Applications to large space telescopes that are planned for future study include the New Worlds Imager (NWI) for Webster Cash. Deploying 35-meter star shades using the foam technology would allow either more NWI telescopes per launch to increase search rates for planetary systems, or a less expensive single launch. The concept is illustrated below:

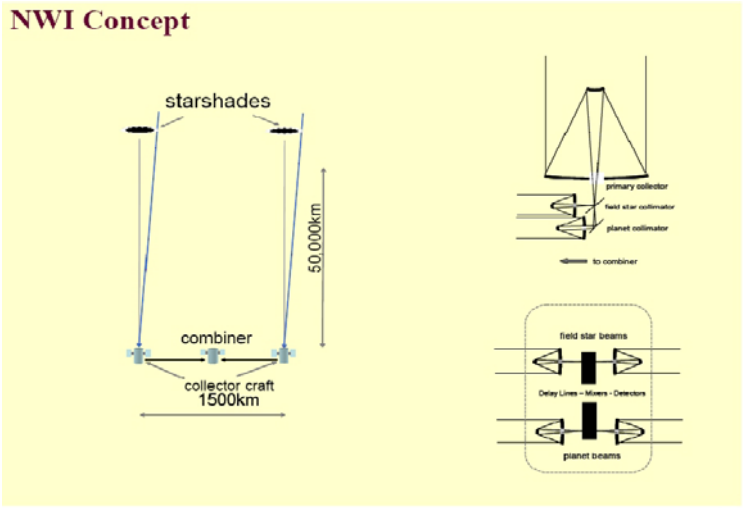

Figure 1. The New Worlds Imager uses star shades for stellar occultation to allow planetary imaging.

A second application of the low mass structures for large telescopes would be the Hypertelescope concept under development by Antoine Labeyrie and his colleagues. In this concept, a dilute aperture interferometer uses pupil densification to concentrate the light into a point spread function (PSF) that approximates that from a filled aperture. The foam technology has sufficient low mass to rigidly locate interferometer elements and thus reduce the burden on station keeping.

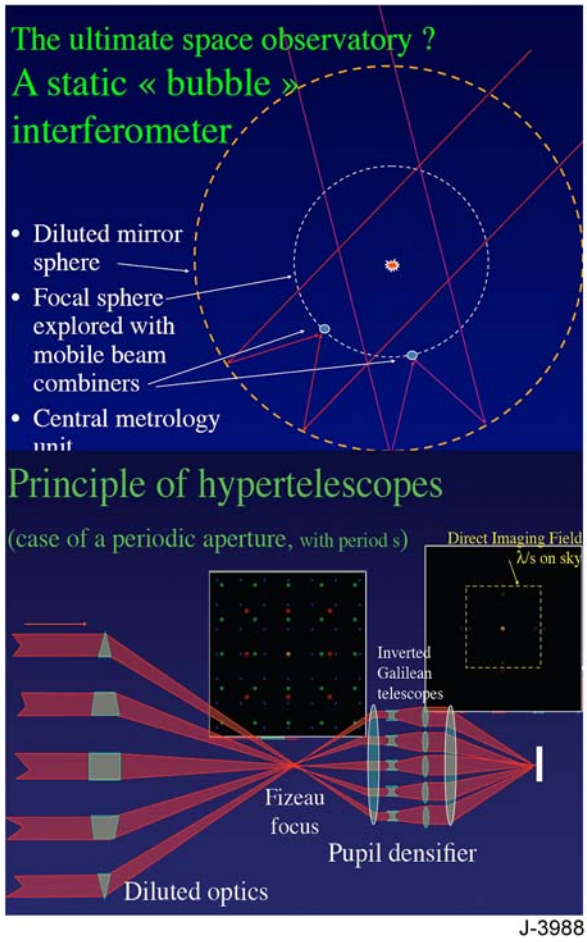

Figure 2. The hypertelscope concept.

Advanced Concept Description

Mass densities in the universe range from black holes to the near vacuum of intergalactic space. Materials that have been used for construction of large structures range from metals to foam insulation or composites such as foam sandwich materials. The mass density of the materials commonly falls with the range of 10 to 0.1 grams per cubic centimeter. The International Space Station total mass divided by the pressurized volume is about 0.35 g/cc. In contrast, the density of a single 70-cm rigid spherical bubble that we have made in a one Earth gravity laboratory environment is about 15 µg/cc. In the microgravity of space, gossamer bubble structures can approach one microgram per cubic meter. We extended this line of thought to

quantify the limits to the size and mechanical integrity of space structures that can be deployed from payloads with launchable mass and volume. We recognize that low mass structures do not include radiation shielding. Small shielded enclosures analogous to the one in the international space station may be needed for manned habitats.

During Phase 1 we will considered methods for creating large structures from small payloads. These methods were analyzed for suitability in each of numerous applications whose requirements were quantified. Examples of applications that this technology could enable include:

- Self-sustaining space habitats for extended duration uses
    - Space stations
    - Planetary expeditions
    - Interstellar voyages.
- Planetary surface buildings.
- Astronomical telescope structures that replace formation flying requirements at very large scales
    - Interferometer arrays
    - Pinhole imagers
    - Long focal length Fresnel plate telescopes
- Large area photon sails, stellar energy collectors, or astronomical primary photon collection surfaces
    - Interstellar photon sailing
    - Solar powered propulsion
    - Laser propulsion at extreme ranges
    - Beamed power transmission
    - Photon perturbation of comet orbits for planetary protection
    - Astronomical research on the origins of the universe and on evidence of life on planets within other solar systems.

Examples of the deployed structure configurations include:

- Orbiting large spheres with multi-kilometer dimensions.
- Domes, or either cylindrical or rectangular prisms, for use as buildings on planetary surfaces.
- Long structural elements to hundreds of kilometers in size and beyond.
- Large area thin walls to tens of thousands of square kilometers and beyond.

Examples of the deployment technologies include:

- Bubble inflation followed by rigidization.
- Frame member inflation followed by rigidization.
- Frame member inflation followed by suspending “soap film” analogs followed by rigidization.

In Phase 1 we quantified structural requirements for each application of interest, then brainstormed and analyzed the lowest mass theoretical solutions for each of those applications. We then explored approaches to engineering the deployment of practical structures. One of the goals for Phase 2 is to create a detailed description of one or more orbital demonstrations of large structural deployment. NASA participation in the selection of applications both for study and for demonstration will be solicited.

A number of bubble-inspired structural designs have been explored, perhaps most notably The Chinese National Swimming Center in Figure 3. This building design exceeds 180-meters on a side with an unsupported roof span on the surface of the Earth. There is also a history of inflated structures in space, including the L'Garde 14-meter microwave antenna that was flown on the Space Shuttle (Figure 4). All of these historical examples have mass densities that, while remarkably low compared to previous practice, do not meet the requirements for the largest scale future applications envisioned in space.

At Physical Sciences Inc. (PSI), we have demonstrated, under government sponsorship, laboratory vacuum chamber manufacture of rigid bubble structures up to 70-cm in size in an Earth-gravity environment (Figure 5). This Earth gravity result would scale up by a factor of 100 to 70 meters in space if the gradient across the bubble was 10^{-4}g. This technology demonstration is an existence proof for processes that can achieve highly precise shapes and rigid structural integrity. Our experience in the precision control of rigid bubble formation gives us a physically characterized experimental baseline for theoretical extensions to very large scale structures made by a variety of bubble technologies. We have also explored the use of low mass large structural rods or towers as supports for an analog to "soap films" as a rigid structural element. We have an ongoing significant DARPA program support for carbon nanotube structural strength enhancement, and we understand both the physical and engineering limitations to low mass structural member fabrication.

The strength of a cellular structure, sometimes called foam, arises from a combination of the aggregated rigidity of the cell boundaries and the net tensile strength of the cell walls. In the National Swimming Center, the cell boundaries are fabricated from steel, and the cell walls are primarily for insulation and appearance. In contrast, the lowest mass density space structures critically depends upon both the bubble interfaces and bubble walls for mechanical integrity. PSI has extensive experience modeling the dynamic and static behavior of mechanical systems using both finite element methods and proprietary software. Cellular structures and frame-supported "soap film" structures are both modeled efficiently using our software tools. In Figure 6, we see that the behavior of foam differs from solid metals as a function of the border-to-interface packing design. For space applications such as habitats, the structure is under internal pressure, and buckling is not as important as the tensile strength of the cell walls. In fact, the internal pressure adds structural integrity. We tailored our aggregates to exhibit the most desirable mechanical characteristics at minimum density. Periodic structures are compared to three-dimensional Penrose tessellations (Figure 7), hyperbolic tessellations (Figure 8), and to both chaotic and random structures. Combined structures is explored that not only mimic well-explored themes such as foam sandwiched between rigid plates, but also combinations of fine foam, coarse foam, aerogels, films, very large bubble cells many meters in extent, and frame augmentation. We quantified the dependence of structural performance upon structural design.

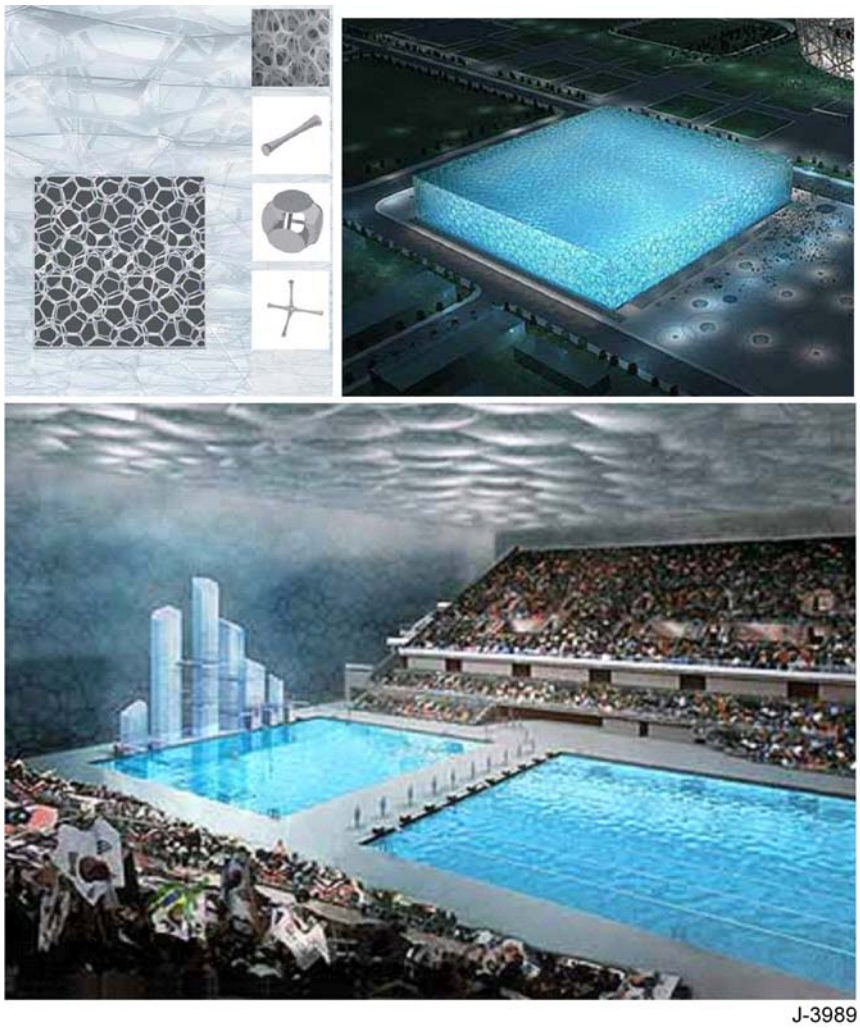

Figure 3. National Swimming Center Design for the Beijing, China Olympics.

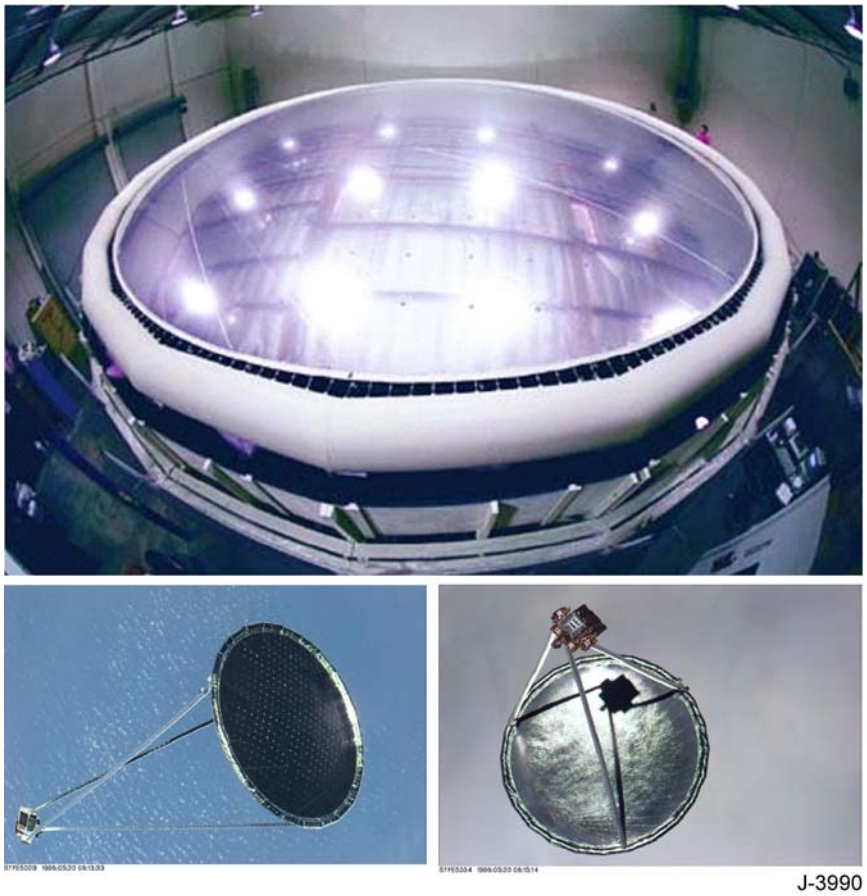

Figure 4. 14-meter L'Garde Inflatable Antenna Space Shuttle Experiment.

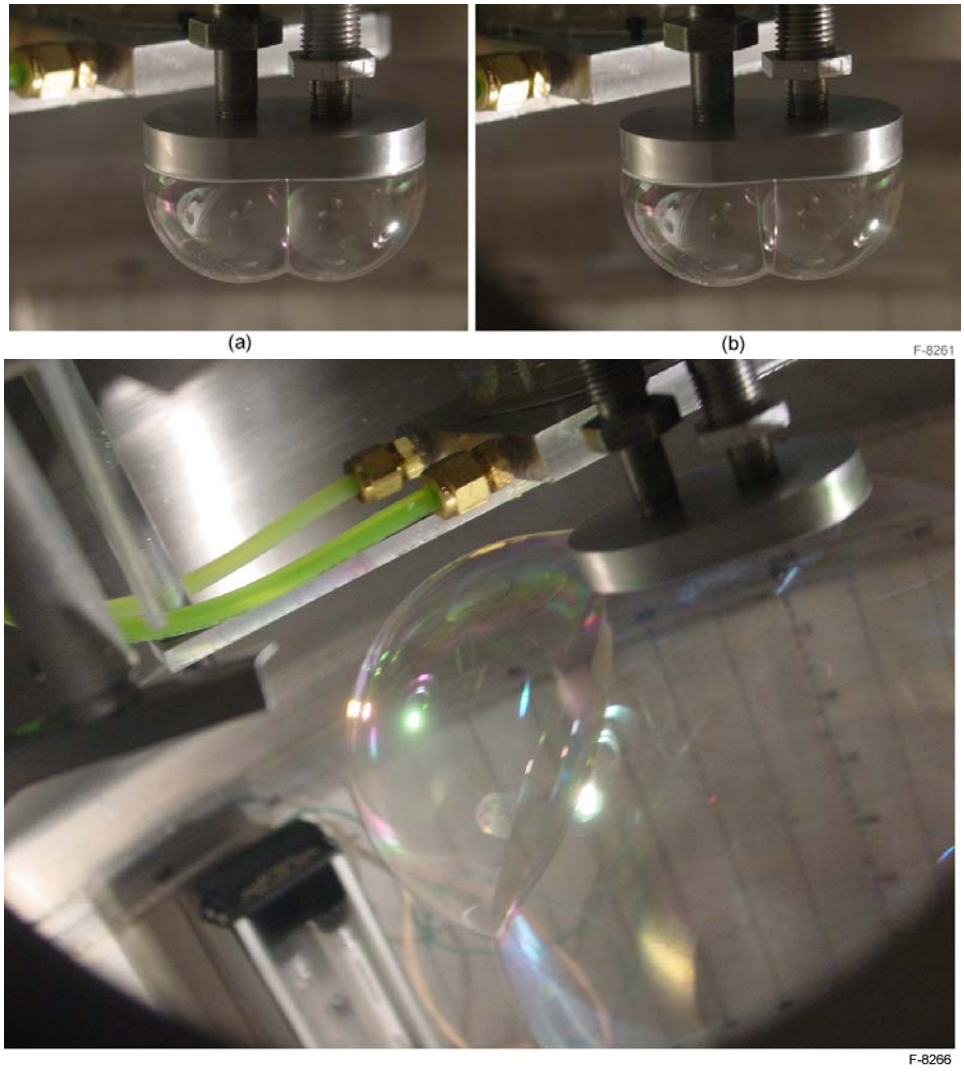

Figure 5. Physical Sciences Inc. has created rigid spherical bubbles with either flat or tailored curved surface interfaces between bubbles in contact. We have demonstrated 70-cm rigid bubbles created in a laboratory vacuum.

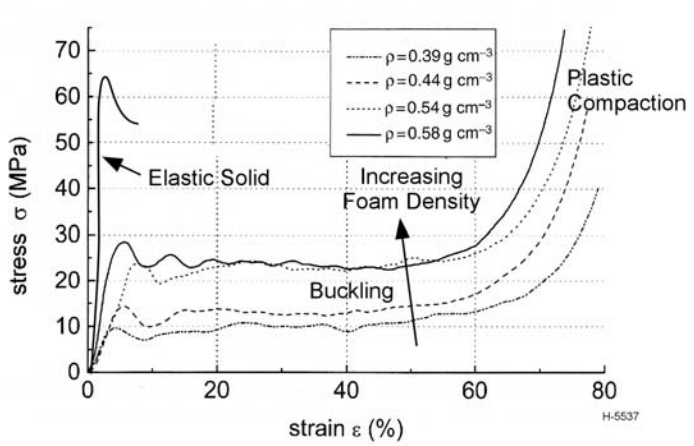

Figure 6. An example of conventional foam design.

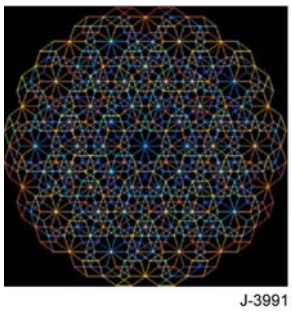

Figure 7. Three-dimensional Penrose volume tessellation.

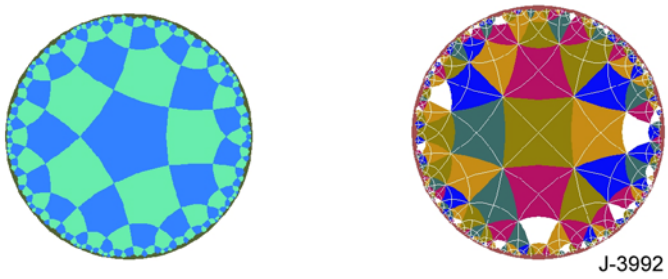

Figure 8. Single and Dual Hyperbolic Tesselations.

Concept of In-Space Fabrication of Large Area Films:

Physical Sciences Inc. developed fabrication techniques for constructing novel large surface area structures in space using UV-rigidizable polymers. Our unique approach can provide large area (~10^4 m^2), ultra-thin (<0.5 micron), ultra-low areal density films (<1 g/m^2) using innovative techniques for (1) forming spherical or planar films from liquid

polymers-surfactants that quickly rigidize under solar UV and (2) achieving high surface reflectivity using aluminum vapor or nanoscale zinc oxide deposition. In-space fabrication of such films can be achieved with reasonably sized space systems.

Consider the example of application of the films to solar sailing, a very promising potential use of highly reflective ultra-thin films fabricated in space. For an 80 kg spacecraft with four 100-m diameter sails (area = 3.5 x 10^4 m^2, mass ~ 30 kg) and ~ 90 kg of sail production materials and mechanisms (jettisoned after sail fabrication), the total launch weight would be ~ 200 kg. The sail loading is ~ 3.5 g/m^2 and the resulting acceleration, ~2.2 mm/s^2, is 6.5 times greater than that for a representative NASA mission[1] with the same spacecraft and launch weights and sail reflectivity (0.85), but with a sail of smaller area (~ 10^4 m^2), greater mass (120 kg), and higher loading (20 g/m^2). In-space fabrication offers a good alternative to the complexity and risk associated with inflatable systems, namely, packaging large, fragile, thin membranes, support structures, and deployment mechanisms into compact stowage[2]. The in-space fabrication approach potentially reduces weight, and increases reliability.

Background:

In the recent years, there has been a resurgence of interest in large distributed aperture space telescopes for earth observation as well as for extraterrestrial planet search. There is also interest in developing spacecraft with in spacecraft equipped with solar sails for monitoring and predicting space weather (e.g., Geostrom)[2,3] as well as for future outer planetary (Titan Flyby) and interstellar (e.g., Interstellar Probe) missions[4]. While the feasibility of various missions employing solar sails had been shown analytically[5], their realization in practice was+ limited by the technology of ultra-thin, lightweight sail materials. The sail subsystem loading (weight including sails, structural hardware, and mechanisms divided by total sail area) for mission of interest to NASA cover the range from <25 g/m^2 for a near-term flight validation mission to ~10 g/m^2 by 2028,[1] Figure 9. The ultimate goal for is ~ 1 g/m^2 for missions beyond the solar system so that the resulting accelerations provide reasonable trip times (a few years) to outer planetary and stellar destinations. The desired range of areal densities for Gossamer telescope applications would also be on the order of 1 g/m^2. Under NASA-funding, SRS Technologies and ABLE engineering company have developed scalable solar sail subsystems that will incorporate a 5-micron CP1 membrane[6] in sails ranging in dimensions from 20 m to 300 m (400 to 90,000 m^2). This design achieves total system loadings (weight of sailcraft, i.e., payload plus spacecraft and its subsystems including the sail subsystem) from ~15 g/m^2 to ~20 g/ m^2 for sail-craft weighing from 50 kg to 100 kg at a sail size of 100 m (sail area 10,000 m^2, see Figure 21 in Ref. 3). L'Garde, Inc. in collaboration with JPL, Ball Aerospace and NASA Langley have reported achieving a sail loading of 14.1 g/m^2 for a 93.3 kg spacecraft (payload and systems) with 47.4 kg sail hardware and inflatably deployed, rigidized booms with a 10,000 m^2 Mylar sail.[7] ***With the fabrication of solar sails in space using rigidizable polymers, we project a sail loading of ~11 g/m^2 for a sailcraft consisting of 100 kg spacecraft and 10 kg of sail hardware with an area of 10,000 m^2.***

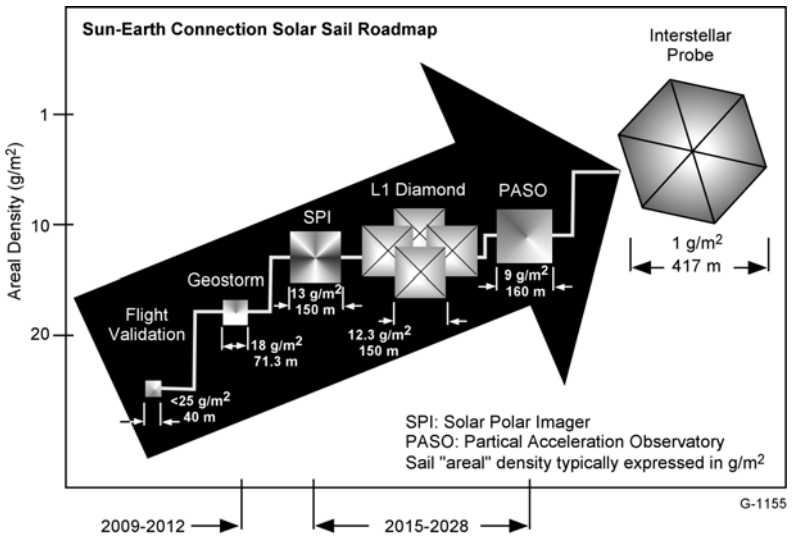

Figure 9. Area Density of Solar Sails Required for Various Missions (courtesy Ref. 1).

An important parameter charactering a solar sail propelled spacecraft is its acceleration, typically expressed in units of mm/s^2. The relationship between ideal acceleration and sail loading (in units of g/m^2) is given by:

$$\text{Acceleration (mm/s}^2\text{)} = 9.12 \text{ /sail loading (g/m}^2\text{)} \qquad (1)$$

where radiation pressure at approximately 1 AU (9.12 μN/m^2) and a perfectly reflecting sail surface are assumed. The ideal acceleration in Eq. (1) is multiplied by a force conversion efficiency, which depends on the sail optical characteristics and on geometrical factors such as billowing and wrinkling of the sail. Values of 0.85 to 0.89 are typical.[5] For insight into the magnitude of acceleration needed for various space missions, reference is made to Figure 10.[5] It is seen that solar sail spacecraft missions to Mercury, Venus, and Mars can be performed within reasonable time for accelerations in the approximate range 0.5 to 2.2 mm/s^2. Also shown in the figure are trip times for missions to outer planets to beyond Mars at 1 mm/s^2 acceleration. ***For the loading of ~11 g/m^2 mentioned above with a space-fabricated, 10^4 m^2 solar sail, the acceleration will be ~0.83 mm/s^2 for a sailcraft mass of 110 kg. With addition of three more sails, each with an area of 10^4 m^2, the spacecraft mass would be 140 kg, the sail loading will be reduced to 3.5 g/m^2, and the ideal acceleration increased to ~2.6 mm/s^2. Assuming a realistic sail reflectance of 85%, the acceleration would be ~2.4 mm/s^2. This is about 4 times the acceleration for the earth-fabricated L'Garde sailcraft (0.58 mm/s^2) in Ref. 7, whose mass (140.7 kg) is very close to our sailcraft mass (140 kg). The calculations illustrate the performance advantages of the proposed ultra-lightweight solar sails fabricated in space.***

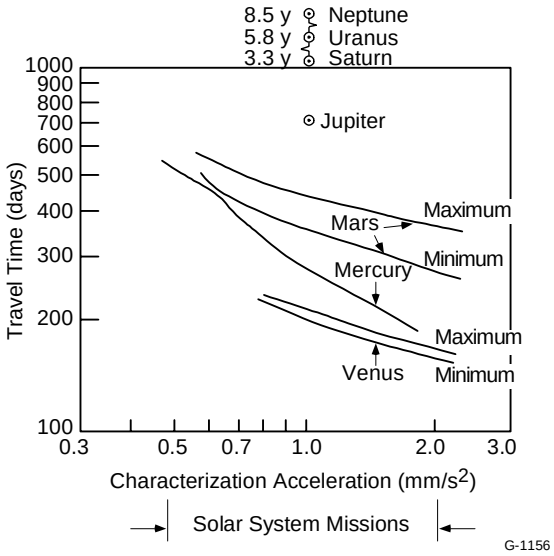

Figure 10. Characteristic acceleration for planetary solar sail missions (from Ref. 7).

The Fabrication Concept:

Our concept of an extremely low areal density (~1 g/m^2) solar sail is based on the work PSI has recently performed for the National Reconnaissance Organization (NRO) to investigate the feasibility of construction of very large area reflective optics in space using rigidizable polymer films.[8] The application of this research was to large aperture, ultra lightweight, earth-viewing telescopes comprising numerous flat primary and curved secondary mirrors. ***Our idea was based on intersecting two spherical liquid bubbles, which form a surface of intersection that is extremely flat if the bubbles are identical in size.*** (If the bubbles are of different diameters, a curved interface is formed.) The concept is illustrated in Figure 11. Due to the surface energy of the liquid, the interface is subjected to circumferentially uniform in-plane tension, resulting in an extremely smooth and very thin (~ micron) film of uniform thickness. If the liquid is a polymer (or a polymer mixture) that is thermally or UV-curable, then the entire system, spheres and interfaces, can be rigidized. ***If this rigidized, ultra-thin, flat surface of intersection can be made highly reflective, it can function as a solar sail or telescope reflector of very low areal density, provided it can be fabricated in sufficiently large area. Large area flat surfaces can be obtained by intersecting very large spheres (~several tens to ~100 meter in diameter). In fact, the unique environment of microgravity makes the formation of very large polymeric bubbles possible.***[8]

On the NRO program[8] we have investigated several UV-curable polymer/surfactant systems. PSI has also developed and made operational a world-class, large vacuum chamber facility (1 m diameter x 1 m high) that is uniquely suited for forming large bubbles, intersecting bubbles, and films. We have developed special techniques for striking films and growing stable bubbles under precisely controlled inflation.

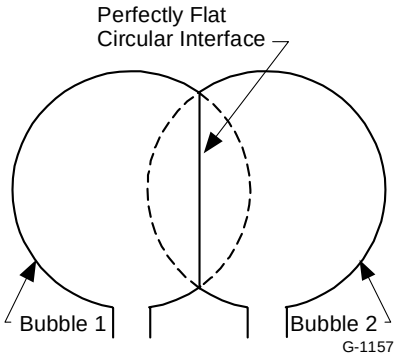

Figure 11. Concept of a flat interface formed by intersecting two spherical bubbles of the same size.

In Figure 12 we show experimental evidence for generating and rigidizing flat surfaces of intersection between two bubbles from our NRO program. For reference, Figure 12(a) shows the familiar illustration of intersection of two soap bubbles (several centimeters in diameter) in bench-top experiments under ambient atmospheric pressure. We note a very flat surface of intersection via the interference patterns that are clearly observed. In Figure 12(b), we show a similar experiment with two polymeric bubbles (a mixture of diisocyanate, polypropylene glycol monomethacrylate and a fluoropolymer surfactant) about 6 cm in diameter formed on a dual shroud in the PSI high vacuum (10^{-6}T) chamber. The inflation of the two bubbles was controlled individually and they intersected at the center of the shroud. The intersected bubbles were then exposed to UV light and rigidized as evidenced by the white strip of cured material around the rim of the shroud.

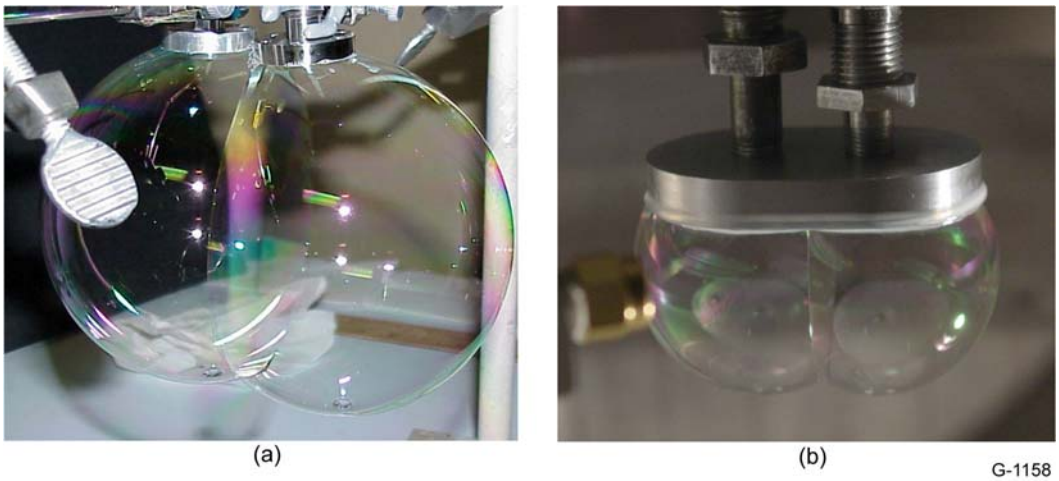

Figure 12. Intersection of soap bubbles and UV rigidization of polymeric intersecting bubbles. (a) Intersecting soap bubbles; (b) Intersecting and UV-cured polymeric bubbles.

In Figure 13, we show a scheme for creating a surface of intersection by passing two polymeric bubbles through two thin wire hoops, rigidizing the entire assembly in UV light, and then cutting away the spherical bubbles on the outside of the hoops. The result is a rigidized flat interface between two wire hoops that act as structural supports. ***This scheme provides one potential approach to fabricating flat solar sail or optical substrates in space by intersecting two bubbles. One of the surfaces can be made reflective by metal vapor deposition as illustrated schematically in Figure 14, where an aluminum pellet is inserted at the center of the rigidized bubble by piercing the bubble wall***. (The inflation pressure within a large bubble in vacuum is already very low, ~10^{-5}T for a ~100 m diameter bubble.) The interior of the bubble essentially acts as a vacuum chamber and the metal vapor condenses on the bubble wall as well as the surface of intersection. Here, the rigidized bubbles provide enclosed volumes for confining the vapor. ***On an Air Force program, PSI has demonstrated the feasibility of creating a reflective bubble by metal vapor deposition on its inner surface.***

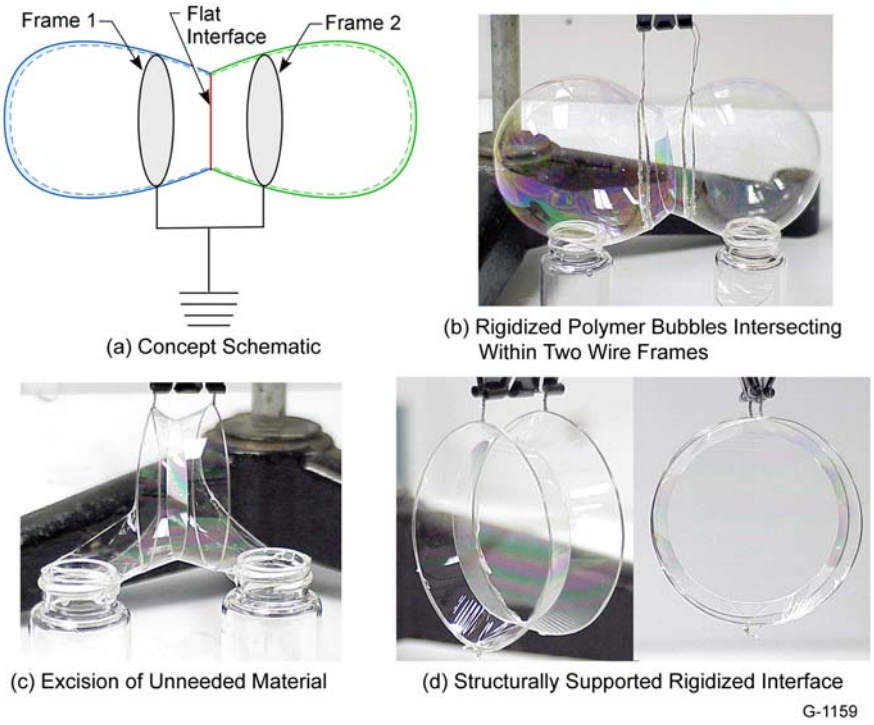

Figure 13. Experimental scheme for fabricating structurally supported solar sails by intersecting and rigidizing two polymeric bubbles passed through two wire hoops.

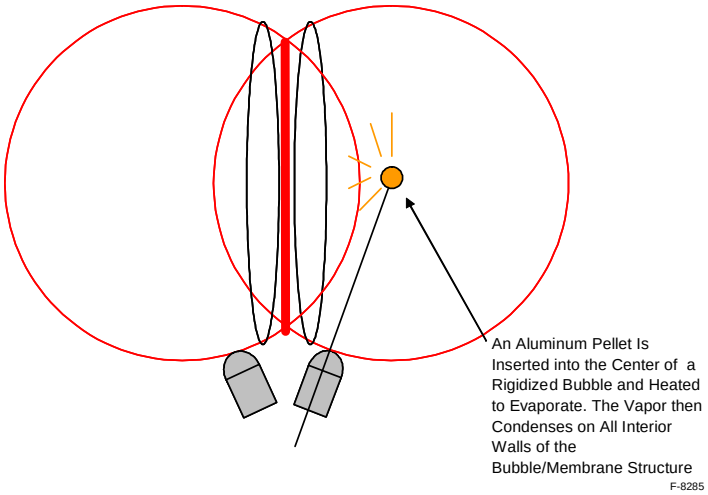

Figure 14. Concept for creating a reflective solar sail by metal vapor deposition.

While the above approach can potentially produce extremely flat and smooth sail surfaces, it has the drawback that a significant amount of polymeric material (as well as deposited metal) is wasted in the excised sections of the two spheres. For example, a 1-micron thick, 100-m diameter polymeric sphere would weigh ~31.4 kg and a 1-micron thick, 50-m disk of intersection between two spheres would weigh only ~3.9 kg. Thus, out of 62.4 kg polymer liquid transported to space, only 7.8 kg would be the useful mass left in the sail, and 54.6 kg or 87.5% mass would be scrap. ***This indicates that it would be significantly more mass efficient to simply make a sail within a large diameter hoop by stretching a polymer liquid film and then rigidizing it. To investigate the feasibility of this approach in Phase II, we will develop for our vacuum chamber facility an experimental flat film fabrication device incorporating an expanding hoop).*** In practice, there is one potential drawback with the approach; metallization (or nanophase particle deposition) of a flat surface, in the absence of a confining bubble, may result in contamination problems. This impact must be carefully assessed for practical applications.

The concept of operations for in-space fabrication of sails or large optics would be as follows. A spacecraft consisting of two main systems, one comprising the payload and spacecraft subsystems and the second comprising sail making equipment and materials, is launched into a parking orbit around the earth. Once the spacecraft and its subsystems are checked out, the sail fabrication process begins. The first step is to form the sails as liquid bubbles/films, which would be done in earth shadow, so that the sails do not rigidize prematurely. As the spacecraft crosses the terminator and enters daylight, the sail rigidization process will begin and be completed in one earth orbit. This will be followed by the process of reflective coatings and excision of any unneeded portions of the bubbles/films. The spacecraft will be equipped with sensors and devices that will ensure that the intended sails have been formed, properly rigidized, and have the required optical properties. At this point, the sail making equipment, leftover materials, and scrap will be jettisoned for deorbit, re-entry, and burn-up in the earth's atmosphere. The smaller spacecraft (now called a sailcraft) and its subsystems will be checked out once again and readied for the long journey to its destination.

PSI has developed a conceptual design for a bubble-making spacecraft and its subsystems under our NRO program.[8] We have shown that a small spacecraft weighing <100 kg would be adequate to carry the supplies and hardware for making ~4 spherical bubbles or ~16 flat sails, depending on the yield of fabrication process.

Effect of Microgravity on Fabrication of Solar Sails:

In the discussion above we referred to very large area spherical bubbles and flat films, tens of meters to ~100 m in diameter. The question arises therefore as to whether such large bubbles (or flat films) can be fabricated in space. How does the microgravity environment affect the ability to form surface tension-driven, large, thin-film structures? We address this question here for the case of spherical bubbles based on the experimental work and analysis performed during the NRO program.[8] We can estimate the largest bubble radius in gravity by balancing the weight of the bubble against the surface tension force along the circumference of the circle that defines the attachment of the bubble to the injection nozzle, Figure 7. The result is the simple relation,

$$R_{b_{max}} = \sqrt{\frac{r\gamma}{\rho g t}} \qquad (2)$$

where r = attachment circle radius, R_{bmax} = maximum bubble radius before rupture, γ = surface tension of polymer liquid, ρ = liquid density, g = acceleration due to gravity, and t = bubble wall thickness. Equation (2) shows that the maximum bubble radius is proportional to the inverse square root of gravity and it is plotted in Figure 15(a) and 15(b) for the cases of earth gravity, 1 g, and microgravity, 10^{-4} g, respectively. We see that ~100 times larger bubbles can be formed in microgravity compared to earth gravity using the same injection nozzle.

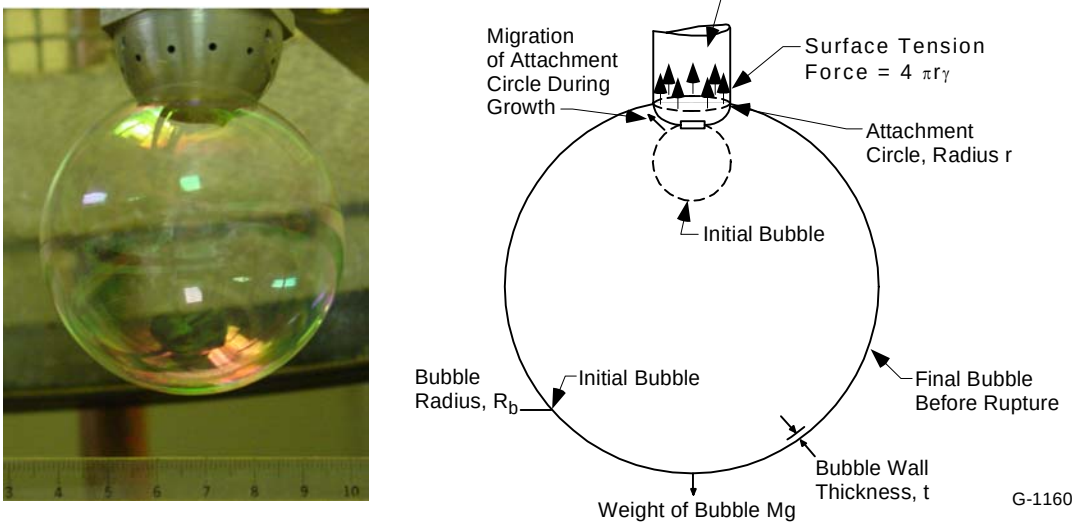

Figure 15. Experimental configuration and model of a spherical bubble under gravity.[8] (a) Bubble formed around injection nozzle in vacuum; (b) Phenomenological model of spherical bubble.

On the NRO project,[8] we used injection nozzles and shrouds that resulted in attachment circle radii from 1.5 to 3.1 cm, which predicts bubble radii in earth gravity of ~30 to 50 cm from Figure 16. This corresponds to bubble diameters of 60 to 100 m in 10^{-4} gravity. Figure 17 shows an example of a 47 cm diameter epoxy bubble we formed in our 1 m vacuum chamber with the 3.1 cm radius shroud.

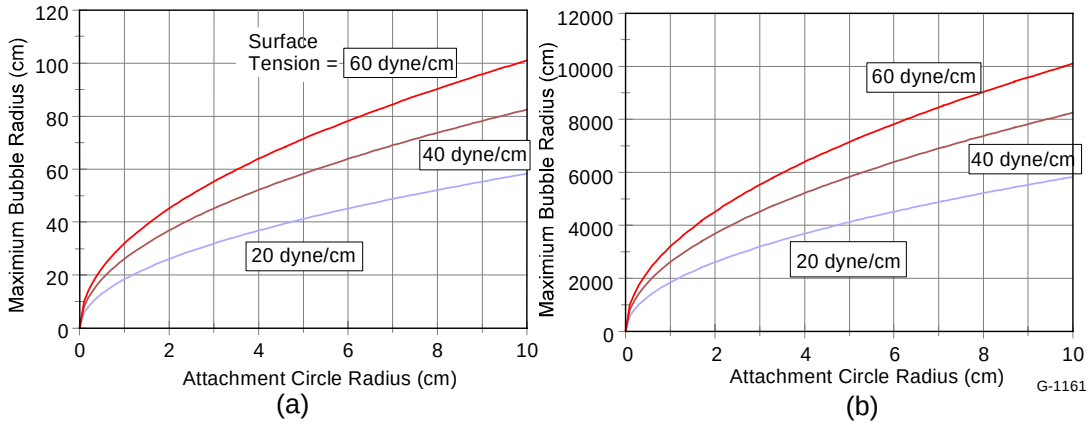

Figure 16. Effect of gravity on maximum bubble size before rupture. (a) Earth gravity (1 g); (b) Microgravity (10^{-4}g)

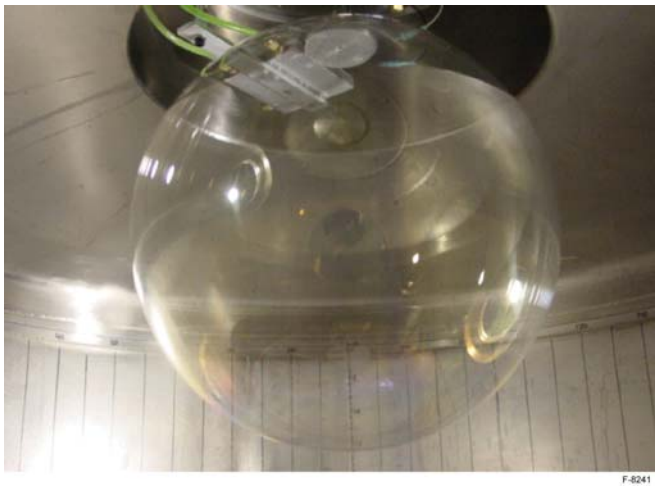

Figure 17. Demonstration of a 47-cm diameter CY179 bubble in PSI 1-m vacuum chamber.

An important issue in formation of thin films and bubbles is their stability, given that the fluid between the inner and outer membranes of the bubble can flow (or drain) under gravitational and thermal gradient driven forces. Thus, the membrane can become thin and ultimately rupture. However, under microgravity, the draining rate is extremely slow.[10] ***As the film thins to micron level values, the fluid velocity is reduced by orders of magnitude (Reynolds number ~ 0), with the result that the currents in the film are practically absent and the film achieves stable equilibrium. At this point, in the presence of UV radiation, the film quickly rigidizes, within minutes as we have demonstrated experimentally.[8]***

The Proposed Solar Sail/Film Optics Configuration Concepts:

In our discussion thus far we have assumed solar sails to be flat disks formed either by intersecting two polymeric bubbles and rigidizing the system or by a directly rigidizing a polymeric film. ***The flat sail clearly possesses the highest propulsive efficiency (for a given solar reflectivity) since the local thrust vector due to photon momentum transfer coincides with the surface normal everywhere on the sail.*** (On a curved sail, components of radiation pressure perpendicular to the direction of incident photons do not contribute to the thrust along the direction of motion.) ***The flat sail is also mass efficient, providing the greatest thrust (radiation pressure times the projected area) per unit mass when compared to a curved surface.*** By comparison, a reflecting sphere is the propulsively four times less efficient than a flat sail of the same radius, R. This is because the thrust developed by the sphere equals the radiation pressure times the projected area πR^2, but its mass is four times that of a flat sail with the same cross sectional area, thickness, and density.

In some cases, however, it may be simpler to form a rigidized, internally metallized spherical bubble from a spacecraft and use it as a sail, Figure 18. This would be the case if the weight of structural supports and other hardware required to fabricate flat sails is comparable to the extra weight of the fluid needed to fabricate a sphere on orbit. For comparison, we show in Figure 19, two flat sails, each with the same radius as the sphere. This sail system is about eight times as efficient as the sphere. Finally, in Figure 19, we show the spacecraft propelled by four circular flat sails, each having the same radius as the sphere. The four flat sail system has the same mass efficiency of the two sail system (ignoring for simplicity overlap between sails).

We now compare the propulsive performance of the sail configurations in Figures 18 through 21 including the mass of the spacecraft propelled by the sails. In Figure 21 we show the sailcraft acceleration (assuming the sail to be a perfect, specular reflector) expressed in mm/s^2 versus spacecraft mass for the four configurations. Each configuration has a sail diameter of 100 m, sail thickness of 0.5 micron, and an overall areal density (including support structure) of $\sim 1\ g/m^2$. Note that the spherical and 4-flat sail configurations have the same mass. Then, for a given spacecraft mass (i.e., given sailcraft mass), the 4-flat sail configuration provides the greatest acceleration, the spherical sail provides the lowest acceleration, with the two-sail acceleration falling in between. As the spacecraft mass increases, i.e., when the sail system mass much smaller in comparison, the acceleration curves asymptote to a constant value and the difference in performance of the three configuration decreases. ***Even then, the simple 100-m spherical sail in Figure 18 provides realistic accelerations for a nanoscale spacecraft, ~ 0.5 mm/s^2 for 50 kg and ~ 1 mm/s^2 for a 25 kg spacecraft. These spacecraft masses are not unreasonable considering the fact that they do not include the sail subsystem masses, which are accounted for separately, and because all the bubble making hardware and polymer supplies are jettisoned once the sails have been fabricated. Thus, the mass of the spacecraft just before it sets sail toward its long distance target is expected to be much lighter than the mass of the spacecraft launched into the parking orbit.***

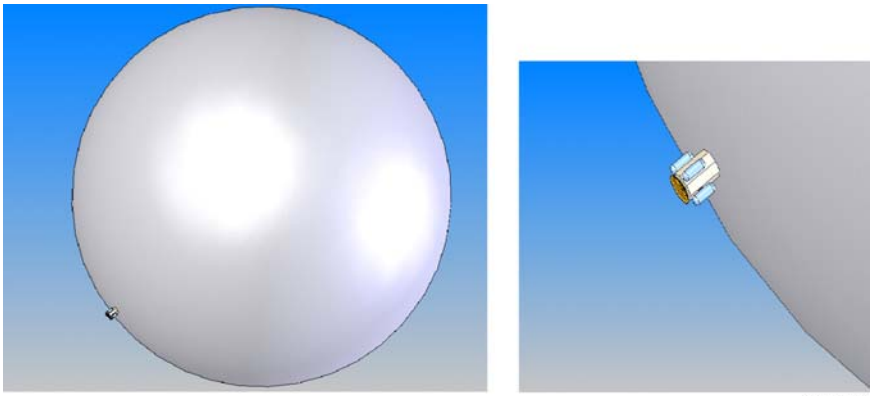

Figure 18. A reflective spherical bubble sail propelling a spacecraft (Bubble diameter ~ 100 m). (The spacecraft is shown 5X larger than scale to aid visualization.)

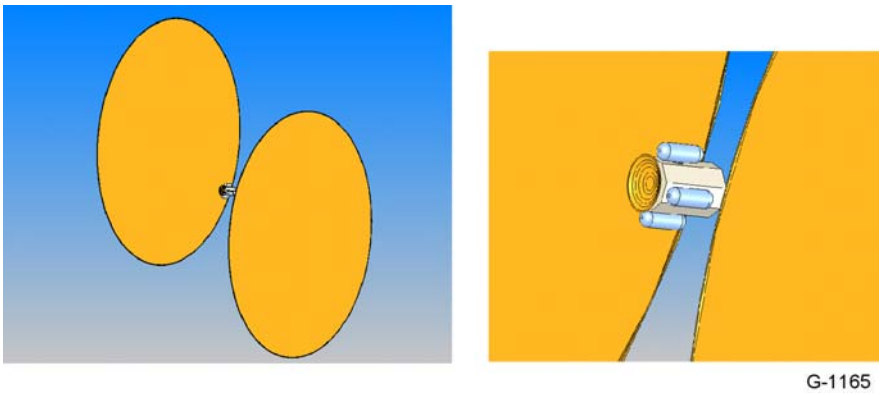

Figure 19. Twin flat sails (~100 m diameter each) propelling a spacecraft. (The spacecraft is shown 5X larger than scale to aid visualization.)

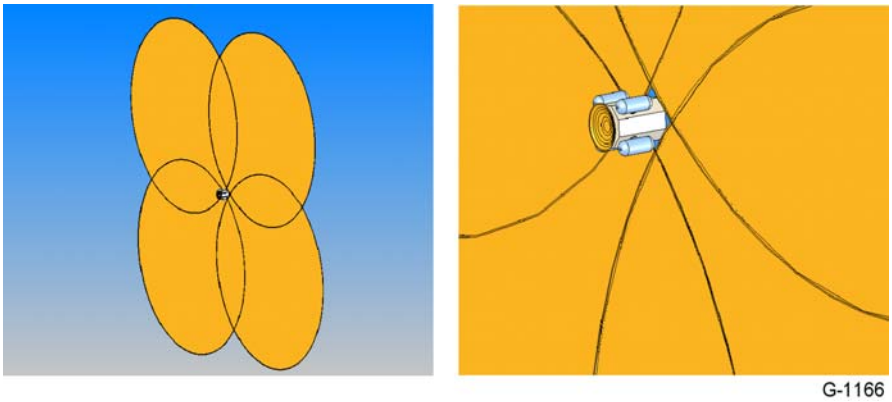

Figure 20. Four flat sails (~100 m diameter each) propelling a spacecraft. (The spacecraft is shown 5X larger than scale to aid visualization.)

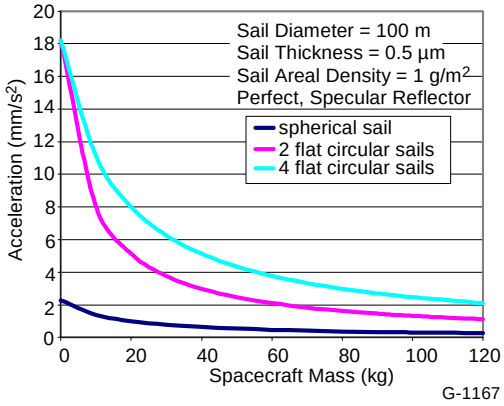

Figure 21. Sailcraft acceleration versus spacecraft weight and sail loading for various sail configurations.

There are many engineering issues associated with the sail configuration concepts shown in Figures 18 through 20. An important question is potential billowing of a sail made from polymeric bubbles and the loss of propulsive performance as a result. ***We have performed preliminary calculations of billowing of a 100-m diameter, 1 micron thick flat sail, prestressed, and rigidly clamped to a hoop. The sail is thus an extremely thin membrane that resists only tension and no compression. We used a NASA GSFC model[9] to determine deflection at the center of a perfectly reflecting membrane under radiation pressure at 1 AU, 9.1 x 10^{-6} N/m^2. Our results show a deflection of 19 cm, which is 0.2% of the sail diameter. Corresponding deflections for a 0.5 and 0.1 micron thick sails are 0.24% and 0.42%, respectively. These deflection values are extremely small and their effect on reducing thrust is negligible.***

To fabricate the flat-films we will develop in Phase II a new film formation device as shown schematically in Figure 22. A linear feedthrough will be used to feed a 5 mm wide (~ 0.1 mm thick) stainless steel ribbon through the device. As the ribbon is fed, it wipes against an aluminum surface loaded with the degassed polymer solution. The emerging wet ribbon carries fresh solution to the film that has formed and is growing. The diameter of the flat-film will increase as the length of fed ribbon is increased. To fabricate a 30 cm diameter flat-film, we must feed approximately 94 cm of ribbon through the flat-film device. We will fabricate bubbles and films of 5, 10, 20, 30 cm diameter and also determine the largest diameter bubble/film that can be grown in our facility.

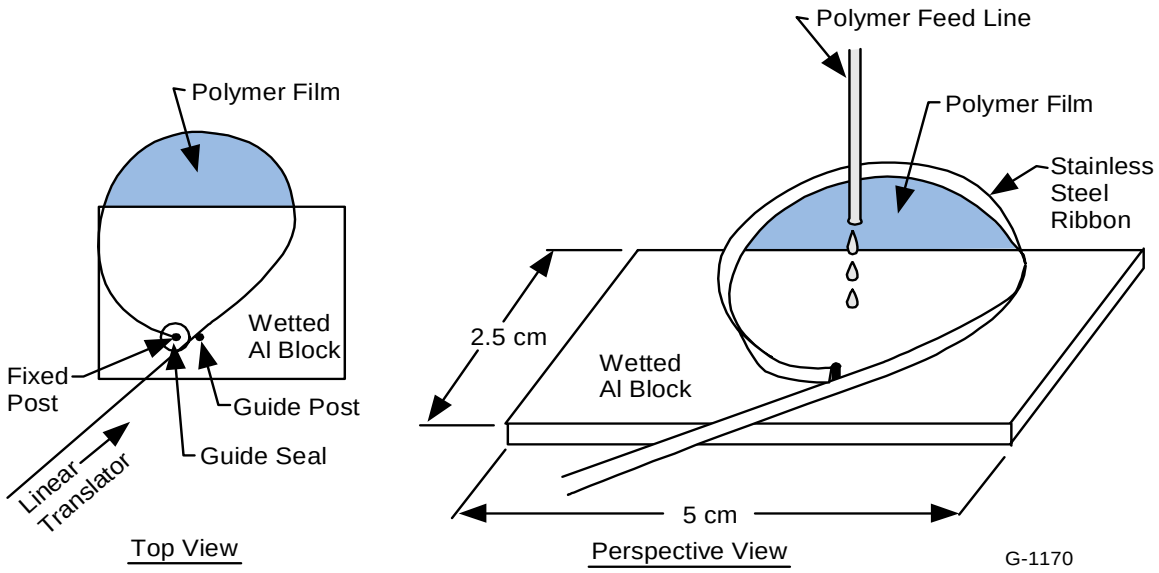

Figure 22. Schematic of the flat-film fabrication device that will be developed in Phase II.

Metallization of Thin Polymeric Films in Space

Both spherical and flat-film cured surfaces (5 cm diameter and greater) will be coated with reflective coatings. Two coating methods will be investigated in Phase II. The first will be metal-film evaporation. An evaporative boat will be set up in the vacuum chamber to coat one side of the films with approximately 100 nm of aluminum. We expect to achieve high quality, specularly reflective coatings by this approach. Although high quality films can be deposited by metal evaporation, this method requires power that must be available on the spacecraft. To provide an alternative method of depositing a reflective coating on the films we will also investigate a method of spraying a reflective coating on the films. In the following paragraphs we describe how we will investigate both approaches.

Metal Film Evaporation

A schematic of the coating apparatus that we will implement in the vacuum chamber for depositing metal films on the thin film surfaces is shown in Figure 23. ***PSI has an operational thin-film coating facility, which includes an evaporative source for depositing metallic films.*** We will use the electrical feedthroughs of this Bell Jar system and its high current power supply for the proposed deposition experiments. The high current (120 V, 40 amp) electrical feedthroughs will be installed onto available ports on the bottom of the vacuum chamber and will be wired to a crucible containing high purity aluminum wire. After the 5-cm diameter polymeric thin-films have been fabricated and cured, they will be positioned above the crucible at the top of a Pyrex chimney that is used to confine the evaporated metal. A Quartz Crystal Microbalance (QCM) will be positioned at the top of the Pyrex chimney to monitor the aluminum film deposition rate and total film thickness during the deposition. We will deposit aluminum films to thicknesses up to 2000 angstroms at rates ranging from 1 to 10 Angstroms/s

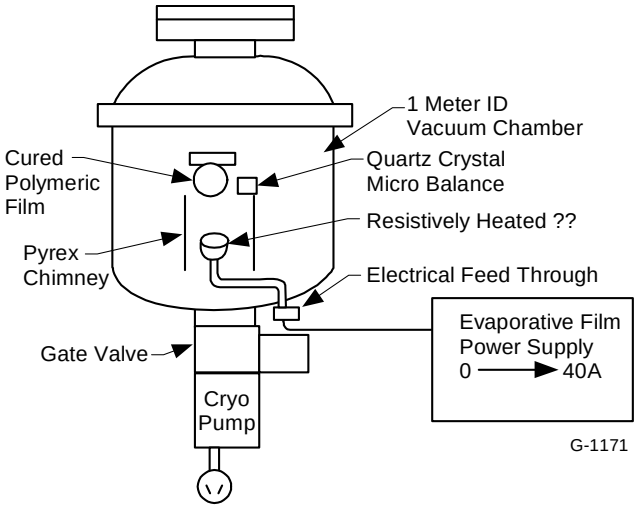

Figure 23. Schematic of the vacuum system configured for depositing aluminum coatings on the thin films.

A summary of the aluminum coating runs that we plan to perform is presented in Table 1. Note that we plan to vary the coating thickness from 100 to 2000 angstroms. Later we will characterize the reflectivity of these films as a function of film thickness. ***We will identify the minimum aluminum film thickness that results in good reflection characteristics. Minimizing the reflective film reduces the time and electrical power required to fabricate the solar sail.***

Table 1. Coating Parameters for the Metal Film Coating Experiments

Parameter	Settings or Range
Coating Thickness	100, 200, 500, 1000, 1500 and 2000 Angstroms
Coating Rate	1 to 10 Angstroms/s

Reflective Spray Coatings

Several space-qualified, highly reflective paints have been developed for thermal control applications on satellites (e.g., Z-93). Many of these paints include particulate zinc oxide in an atomic oxygen resistant binder such as potassium silicate. The reflective nature of these paints suggests that they may be useful as an easily applied reflective layer on solar sails. However, such paints are unsuitable for direct application to our thin-films (typically 0.5 to 1.0 μm thick) because a single coat of the paint would be likely to be at least an order of magnitude thicker (and heavier). We therefore propose to coat our thin film surfaces directly with commercially available nanophase zinc oxide powder (~ 20 nm diameter) that has been dispersed in a high vapor pressure solvent such as methanol. As the zinc oxide/methanol mixture is spayed onto the thin-film surface in the vacuum chamber, the methanol will quickly evaporate leaving the dry oxide powder to deposit on the cured polymer surface. To promote adhesion of the zinc oxide powder onto the thin-films, for these experiments we will only partially cure the IPDI/PPGMM and CY179 films so that they remain tacky.

A schematic of the spray coating system that will be implemented in the proposed effort is shown in Figure 24. ***We will use bell jar vacuum system available at PSI to deposit the spray coatings onto 5 cm diameter, cured flat-films.*** The flat films will be positioned in the Bell Jar below a SonoTek™ ultrasonic sprayer. The solution of nanophase zinc oxide dispersed in solvent will be dispensed through a syringe filter to the sprayer. The effect of spray solution concentration, the sprayer to thin film distance, the solution feed rate, and the coating thickness on the quality of the sprayed-on coatings will be evaluated. Our goal will be to achieve uniform, approximately 1000-angstrom thick adherent coatings on the flat-films.

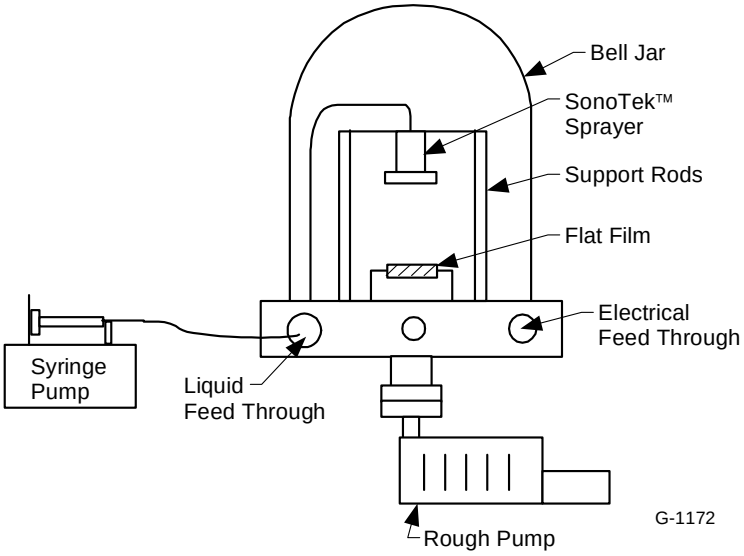

Figure 24. Schematic of the spray-coating system that will be used in Phase II to apply the nanophase zinc oxide coatings.

The critical issue in vapor deposition on a ~1-micron thick polymer film is heat transfer as a result of phase change of particles from vapor to solid. The concern is that this local heat transfer will melt the film. This heat is added to the film material as it is radiating to the space environment. The calculation in Figure 25 from our NRO program[15], which includes earthshine from a 270 K blackbody, shows that at a deposition rate of 7 angstrom per cm^2 per second, a spherical bubble will equilibrate to 275 K. In the aluminum vapor reflective coating experiments discussed above, we have proposed a deposition rate of 0.05 to 0.5 angstrom per cm^2 per second for a 5 cm diameter film. Our experimental measurements of reflectivity versus deposition rate will provide the lowest deposition rate necessary to obtain high reflectivity for sail performance. We must optimize the deposition rate so that coating over a very large area (~10^4 m^2) is completed within a reasonable time with the high reflectance necessary for sail performance. Our model will be modified to aid in this optimization.

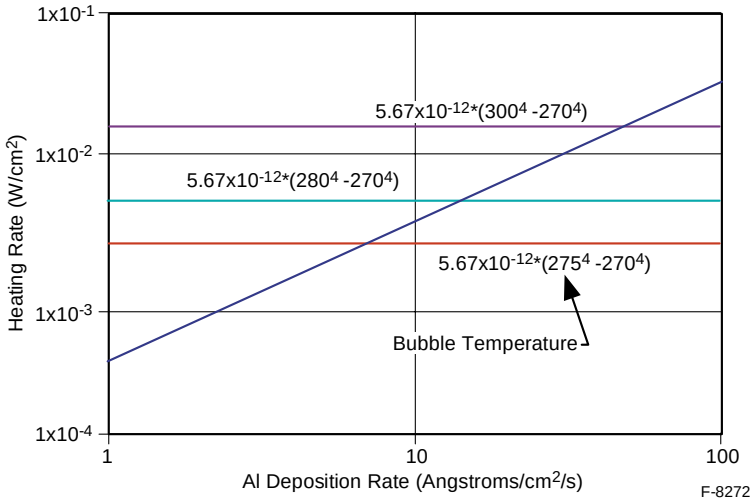

Figure 25. Equilibrium temperature of a spherical bubble in LEO thermal environment as a function of aluminum vapor deposition rate.[8]

Mechanical and Optical Characterization of Films

Mechanical characterization

We will evaluate the mechanical strength of selected flat-films by attaching the film and its metal ribbon frame to an aluminum plate as shown in Figure 26. The metal ribbon will be glued to the plate with epoxy to establish a gas-tight seal. The plate will include a port for measuring the pressure in the sealed region defined by the flat film. Pressure will be measured with a baratron. Gas will be slowly (1 to 10 sccm) added to this volume at a measured rate controlled with a needle valve. For a 30 cm diameter flat film, the reservoir volume will be approximately 140 cm^3. A gas flow rate of 1 sccm will therefore raise the reservoir pressure by 1 Torr in approximately 11 seconds. The pressure and deflection height will be monitored versus time for a constant gas flow rate. The pressure (N/m^2) corresponding to a break in the linear increase in the pressure of the reservoir will determine the applied force at failure. A plot of film stress versus stain (determined by the film deflection height) will be made to evaluate yield strength of the film. After each experiment, the films will be inspected to identify their failure point (e.g., at the interface with the metal strip or in the film itself).

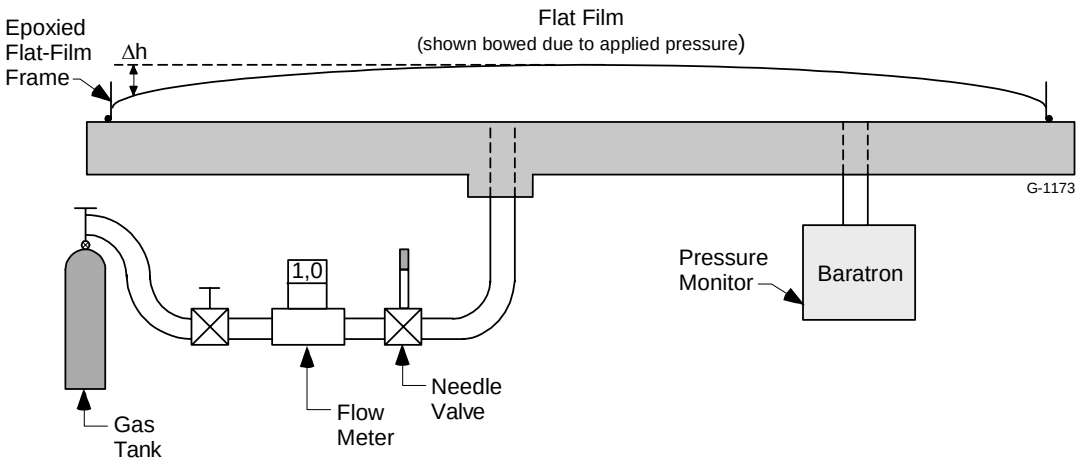

Figure 26. Schematic of the experimental set-up for evaluating strength and failure mechanism(s) of cured thin films.

Optical characterization

The reflectance spectrum of selected coated flat-films will be evaluated from 200 to 3.0 microns using our Shimadzu 3100UV spectrophotometer with an integrating sphere attachment. This system will measure the reflectance spectrum from both specular and diffuse reflective surfaces. (The Shimadzu will also be used to estimate thicknesses of uncoated films by transmission measurements.) The specular scattering characteristics of selected films will also be evaluated. A HeNe laser (632.8 nm) will be scattered from the films at an incident angle of 45 deg with respect to the films surface normal and the scattered light intensity will be measured as a function of angle around the specular angle using a silicon photodiode detector available at PSI. ***The reflectance spectra and the degree of specularity of the reflection will be used to calculate the propulsive performance of solar sails fabricated from the thin-film material.***

Space system concept for fabricating flat sails

The concept for an apparatus for forming flat membranes in space is shown in Figure 27. It consists of a spool of special ribbon and a membrane-formation block. The ribbon incorporates a stripe down its center, which is coated with a material that promotes wetting by the membrane-forming polymer liquid. The liquid is fed though the entry port in the back of the block and into the membrane feed groove in the front of the block. As the ribbon is fed into the block, a loop of expanding diameter is formed with a membrane across the center of the ribbon as shown in Figure 27.

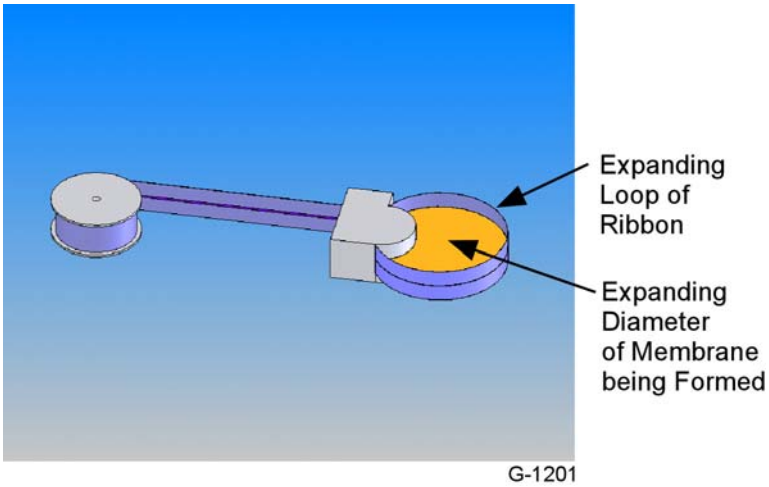

Figure 27. Concept of an expanding loop mechanism for forming membranes for solar sails.

The concept in Figure 27 will be further developed to evaluate its implementation as a space system. The data from the expanding hoop film experiments will be the inputs. We will identify the tape feeding rates, system components, estimate the weight and power required, and develop conceptual designs.

We will also develop the concept for metallizing large area (~100 m diameter) flat sails by vapor deposition. We will extend the concept for metallizing the spherical bubbles shown earlier in Figure 13. Our initial thinking is that two flat films will be held closely together and a long (~50 m) telescoping rod, carrying an electrically-heated reservoir of aluminum, will be inserted between them. However, we must address the issues of coating uniformity and the need to avoid escaping aluminum vapor. We will identify the system concepts including mechanisms, and estimate the weight and power.

Bubble and flat sailcraft system concepts

We will develop in Phase II sailcraft concepts incorporating spherical and flat sails as depicted in Figures 18 through 20. The very low areal densities that result from the use of space-fabricated thin polymeric films provide important performance advantages for a wide range of solar sailing missions. It is essential that the sailcraft bus concept and sail support structure effectively combine to realize these performance advantages. We will investigate at the concept level the sailcraft design, its performance level, its stability and controllability, and its methods of operations. The concept design will include methods of attachment of the sails and their ring structures, identification of sail movement requirements (as for balance and control), and specific methods of obtaining attitude control. The effects of sail curvature on performance and control will be evaluated using FEA software previously developed by Jerome Wright specifically for solar sailing spacecraft.

The sail-support rings will attach to the sailcraft bus through 1- or 2-degree-of-freedom joint mechanisms. The mechanism structures will carry force and torque loads from the sails to

the sailcraft bus. The mechanisms will be designed to carry the force and bending loads while providing necessary joint motions. These mechanisms are expected to provide full balance and control of the sailcraft and thus avoid a requirement for separate control vanes. As an alternative method of control, a center-of-mass balance arm will also be evaluated for use with the sails. Another method of control will be to use a control moment arm that provides separation and articulation between the bus and the sail assembly.

Summary

We have described the Phase 1 effort and planned future work:

- Deployment of Rigid Bubbles has been demonstrated in the laboratory
  - Spheres
  - Flats
  - Curved surfaces
  - Theoretically Scalable to 100 km single bubble in low earth orbit
  - Theoretically Scalable to 1,000 km single bubble in deep space
  - Foam structural element span can far exceed single bubble in extent
- Suitability for selected missions has been analyzed
  - Solar sails
  - Extra solar planet imaging telescopes
- We propose to design missions in Phase 2 that could fly in the 2020 to 2030 mission planning period
  - New Worlds Imager (Web Cash)
  - Maxim (Web Cash)
  - Hypertelescope embodiments
  - Solar Sails
- We propose to demonstrate laboratory feasibility of miniature mission prototype structural elements and optical surfaces

References

1. Garbe, Gregory and Montgomery, Edward, "An Overview of NASA's Solar Sail Propulsion Project", AIAA Paper 2003-5274, 39th AIAA Joint Propulsion Conference, Huntsville, Alabama, July 20-23, 2003.
2. Wright, T., Laue, G., and Horner, G., "A Practical Approach to Large-Area Solar Sail Assembly Utilizing the Miura-Ori Folding Technique" AIAA Paper 2003-4663, 39th AIAA Joint Propulsion Conference, Huntsville, Alabama, July 20-23, 2003.
3. West, J.L. and Derbes, B., "Solar Sail Vehicle Design for the Geostorm Warning Mission", AIAA Paper 2000-5326, 41st Structures, Structural Dynamics, and Materials Conference, Denver, CO.
4. NASA SBIR and STTR Program Solicitations, Topic S1.02, Deep Space Propulsion - Solar Sails, July 2003.
5. Wright, J.L., Space Sailing, Gordon and Breach Science Publishers, Philadelphia, 1992.

6. Murphy, D.M. and Murphey, T.W., "Scalable Solar Sail Subsystem Design Considerations", AIAA Paper 2002-1703, 43rd Structures, Structural Dynamics, and Materials Conference, Denver, CO, 22-25 April 2002.
7. Lichodziejewski, D., Derbes, B., West, J., Reinart R., Belvin, K., and Pappa, R., "Bringing an Effective Solar Sail Design Toward TRL 6", AIAA Paper 2003-4659, 39th AIAA Joint Propulsion Conference, Huntsville, Alabama, July 20-23, 2003.
8. Joshi, P., Oakes, D., Salley, E., Gelb, A., Hagge, J., Green, D., and Lester D, "Microgravity Fabrication of Large Area, Ultra Lightweight, High Precision Mirrors for Very Large Aperture, Earth-Viewing Systems, Final Report submitted to the National Reconnaissance Organization, August 22, 2003.
9. Deflection of Stretched Circular Membrane Under Pressure, NASA Techbrief, Goddard Space Flight Center, September 1999, http://www.nasatech.com/Briefs/Sept99/GSC14223.html
10. Isenberg, R., The Science of Soap Films and Soap Bubbles (TIETO Ltd., 5 EltonRoad, Clevedon, Avon, England, 1978).
11. Salama, M., McInnes, C., and Mulligan, P., "Gossamer Sailcraft Technology", in Gossamer Spacecraft: Membrane and Inflatable Structures Technology of Space Applications, Chapter 19, Jenkins, C. Ed., Progress in Astronautics and Aeronautics, Volume 191, American Institute of Aeronautics and Astronautics, 2001.

Figure Addendum: A Really Large Set of Bubbles

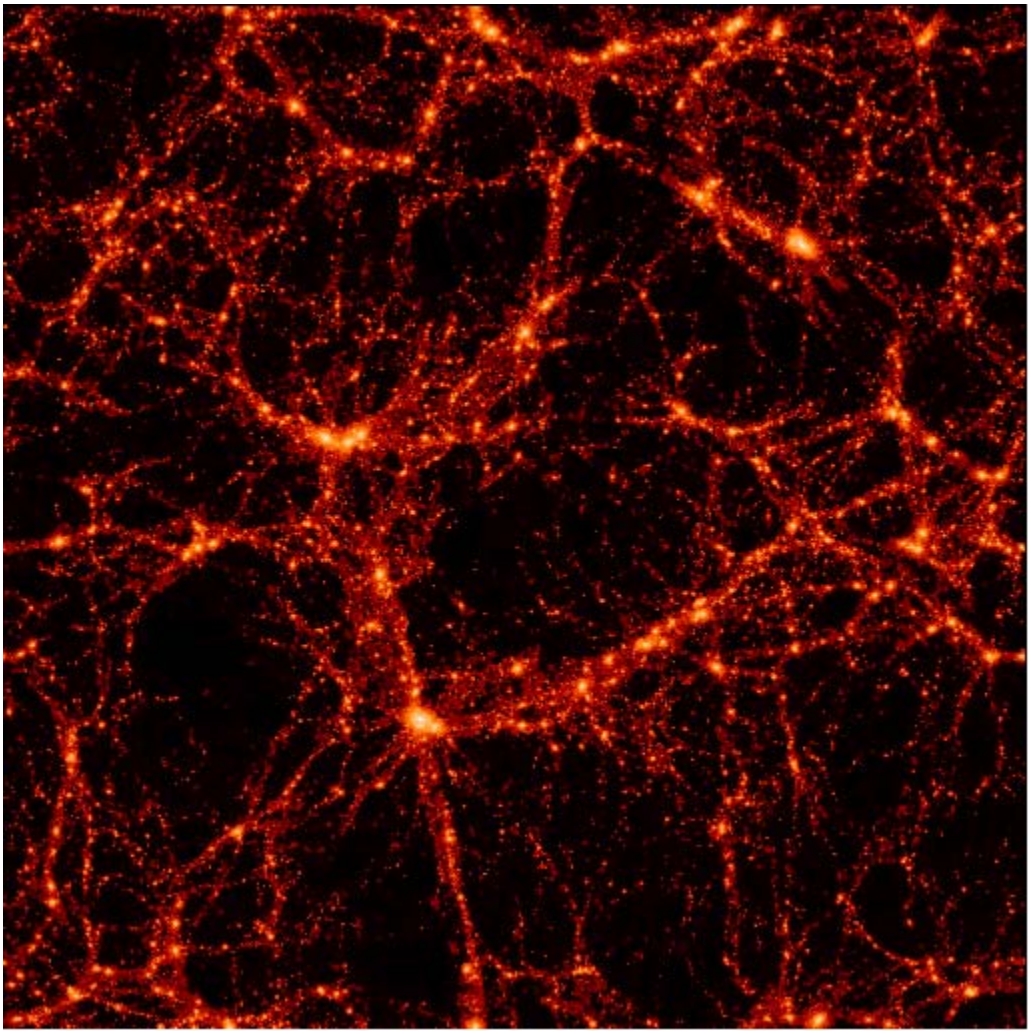

"This is a computer simulation of the large-scale structure of the Universe, created by a group of scientists known as the Virgo Consortium. The box 'measures' 300 million light years on a side. The big bright spots are clusters of galaxies, while the smaller dots represent individual galaxies and groups of galaxies. The knot near the lower center of the picture appears to be what we believe is a good representation of the merger system Abell 754. The filamentary structure of the Universe is apparent, and we believe that mergers happen at the intersection of the filaments. In some sense the merging clusters 'hit' each other at these locations. Credit: The Virgo Consortium."
Credit: http://www.nasa.gov/centers/goddard/news/topstory/2004/0831galaxymerger_media.html